Journal of Mineralogical and Petrological Sciences, Volume 112, page 291–299, 2017

Cathodoluminescence petrography of P-type jadeitites from the New Idria serpentinite body, California

Naoko TAKAHASHI[*], Tatsuki TSUJIMORI[*,**], Masahiro KAYAMA[*,***] and Hirotsugu NISHIDO[†]

[*]*Graduate School of Science, Tohoku University, Aoba, Sendai 980-8578, Japan*
[**]*Center for Northeast Asian Studies, Tohoku University, Aoba, Sendai 980-8576, Japan*
[***]*Creative Interdisciplinary Research Division, Frontier Research Institute for Interdisciplinary Sciences, Tohoku University, Aoba, Sendai 980-8578, Japan*
[†]*Department of Biosphere-Geosphere Science, Okayama University of Science, Okayama 700-0005, Japan*

Jadeitite from the New Idria serpentinite body of California is a fluid precipitation-to-metasomatic product. Optical cathodoluminescence (CL) microscopy of the jadeitite revealed that vein-filling 'pure' jadeites (mostly 97–99.9 mol% jadeite) exhibit bright luminescence, whereas 'impure' jadeites (mostly 75–95 mol% jadeite) in pale-greenish matrix show dark luminescence. The 'pure' jadeites in the veins are composed of mixtures of red, blue and dull blue CL-colored domains, showing growth textures (oscillatory bands). The 'impure' jadeites in the pale-greenish matrix with dark luminescence have a higher augite component (up to 5.37 wt% FeO), implying that the CL property is due to significant amount of Fe^{2+} to act as a quencher. CL spectra of the blue CL-colored domains of the vein-filling 'pure' jadeite have a doublet broad emission peak centered at ~ 320 and ~ 360 nm in the ultraviolet (UV) to blue region. In the red CL-colored domains, a broad asymmetric emission peak at ~ 700 nm is also recognized together with the doublet UV-blue emission peak. Comparing monochromatic CL images in the UV-blue (300–400 nm) and red (650–750 nm) emission regions with X-ray elemental maps, luminescence centers contributing the UV-blue and red CL emission peaks were assigned. The red emission peak of the 'pure' jadeite with subtle augite component would be attributed to lattice defects related to Ca^{2+}, Fe^{2+} (or Fe^{3+}) and Mg^{2+} deficiency and/or excess centers in M1 or M2 sites. Alternatively, transition metal ions (Mn^{2+} and Fe^{3+}) or rare earth elements in the M1 and M2 sites as impurity centers, might contribute to the red emission peak. As the UV-blue emissions correlate with Al^{3+} content, i.e. purity of jadeite component, they might be related to Na^{+} and/or Al^{3+} defect centers.

Keywords: P-type jadeitite, Jadeite, Cathodoluminescence, Spectroscopy, New Idria serpentinite body

INTRODUCTION

Cathodoluminescence (CL) is a powerful tool in petrology and mineralogy for observing internal texture of specific minerals (e.g., zircon, plagioclase, fluorite, calcite, diamond, SiO_2, and Al_2SiO_5 polymorphs) (e.g., Marshall, 1988; Götze et al., 2000; Steaven-Kalceff et al., 2000). Recently, optical CL microscopy has been applied to jadeitic clinopyroxenes in jadeitite to visualize growth and overgrowth textures (e.g., Sorensen et al., 2006; Schertl et al., 2012); the CL image easily provides valuable information on subtle stepwise compositional differences of the jadeitic clinopyroxenes, as a variation of CL brightness and color, which are generally invisible under crossed-polarized views of an optical microscope (Schertl et al., 2012). In general, CL features of minerals, such as brightness and color, are contributed by the existence of luminescence centers. The luminescence centers are divided into intrinsic and extrinsic centers. The intrinsic centers include lattice defects caused by non-stoichiometry or structural imperfections, whereas the extrinsic centers are attributed to impurities such as transition metal ions (Mn^{2+}, Fe^{3+}, and Cr^{3+}) and rare earth elements (REEs). In either case, concentration and elemental species of the luminescence centers depend on physico-chemical conditions during crystallization or recrystallization of the luminescent minerals (Marfunin, 1979; Yacobi and Holt, 1990; Götze et al., 2000; Steven-Kalceff et al., 2000, Vasyukova et al., 2013). Based

doi:10.2465/jmps.170403
N. Takahashi, naoko.takahashi.t1@dc.tohoku.ac.jp Corrresponding author

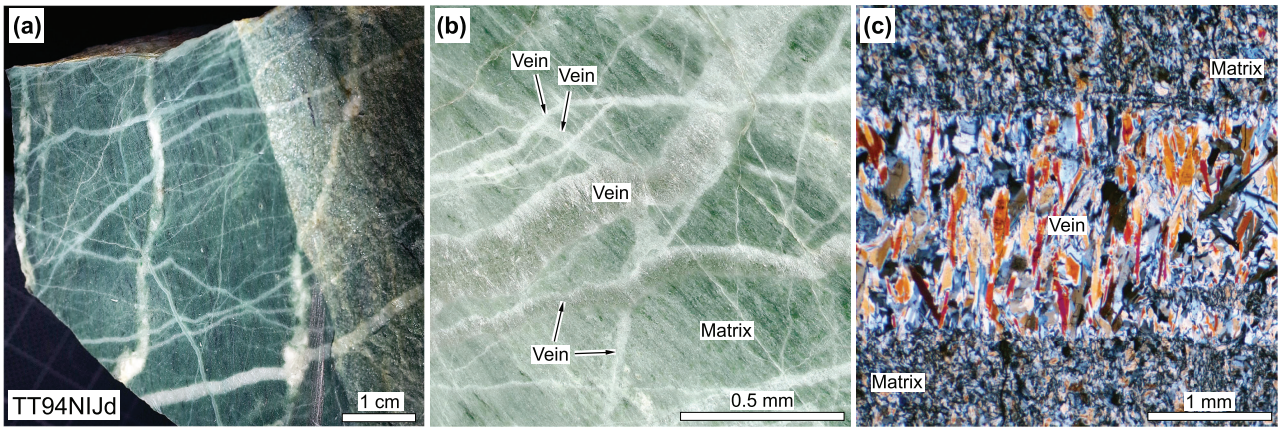

Figure 1. (a) Photograph showing the polished surface of investigated jadeitite (TT94NIJd) from the New Idria serpentinite body. Note that pale-greenish jadeite matrix cut by white veins. (b) Optical image of a polished thick section of the sample, showing cross-cutting relationships between the matrix and multiple veins. (c) Photomicrograph of a jadeite vein crosscutting fine-grained jadeite matrix (crossed-polarized light view). The vein consists of coarser-grained jadeites, which tend to be oriented perpendicular to the vein walls.

on optical CL features of jadeite crystals in jadeitites, Sorensen et al. (2006) have successfully defined the relative order of jadeite crystallization. Obviously, these observations promised new insights into interpretation of multiple sources and generations of the jadeite-forming fluids. Nevertheless, the mechanism of CL emission in jadeite and featuring color variation is still unclear.

In this study, we performed CL microscopy and spectroscopy combined with electron probe microanalyser (EPMA) analysis for a P-type jadeitite (jadeites directly crystallizing from H*P*-L*T* aqueous fluids: Tsujimori and Harlow, 2012) from the New Idria serpentinite body of the Diablo Range (California, USA). Sorensen et al. (2006) reported that jadeites in the New Idria jadeitite show only red and blue CL, although the jadeitites from the other localities consist of red, blue, and green CL-colored jadeites. We further describe internal textures and chemical variations of the red and blue CL-colored jadeites in the New Idria jadeitite using both CL microscopy and spectroscopy, together with elemental analysis, to characterize the luminescent features with interpretation of luminescence centers.

GEOLOGICAL OUTLINE

The studied jadeitite was collected from the New Idria serpentinite body (NISB), in the southern extension of the Diablo Range of the California Coast Ranges between the San Andreas fault on the west and the San Joaquin Valley on the east. The serpentinite body (~ 23 × 8 km) is in contact with the Franciscan Complex (Jurassic and Cretaceous), the Panoche Formation and the Moreno Formations of the Great Valley Group (Late Cretaceous); the contact is marked by high-angle faults and/or shear zones (Coleman, 1961, 1986; Vermeesch et al., 2006). The NISB is considered as an on-land analogue of active serpentinite diapirs containing exotic blocks of blueschist- and eclogite-facies rocks (Tsujimori et al., 2007). The presence of active landslides on the flanks of the serpentinite body (Cowan and Mansfield, 1970) and the deposition of detrital serpentinite in terrace deposits as young as 500 yr B.P. (Atwater et al., 1990) are also strong evidence that the NISB continues to rise. Fission track thermochronology of detrital apatite from the Great Valley Group forearc sediments suggested the rapid rise of the NISB as a heat source (T > ~ 110°C) to anneal apatite fission tracks at ca. 14 Ma (Vermeesch et al., 2006). The NISB is supposed to rise as serpentinite diapir from mantle depths and enclosed tectonic blocks at various mantle-crustal levels during upwelling by the wide range of P-T conditions of tectonic blocks (Tsujimori et al., 2007).

SAMPLE DESCRIPTION

The selected samples (TT94NIJd) are fine-grained jadeitites with pale-greenish in color cut by subcentimeter to submillimeter wide veins of white colored jadeites (Fig. 1). They were obtained from a tectonic block (~ 1 × 5 m in size) enclosed by a serpentinite-matrix near Clear Creek of the NISB. The samples are massive, but exhibit a weak foliation defined by parallel alignment of subtle color changes in the pale-greenish matrix. The pale-greenish matrix is composed mostly of fine-grained and well-recrystallized jadeites. In some cases, the matrix contains somewhat porphyroclastic coarse-grained jadeite grains. The samples are also characterized by multiple generations of white colored jadeite veins (less than ~ 2 mm). The veins consist of coarse-grained subhedral jade-

ites (~ 100-500 × 50 μm). Texturally, these vein-filling jadeites are newly precipitated crystals in microfractures. The vein-filling jadeites tend to be oriented perpendicular to the vein walls. Relatively coarse-grained jadeites in a few veins of older generation represents a disrupted texture due to a deformation after the formation of these veins. Two-phase fluid inclusions ($H_2O + CH_4$) are ubiquitous in the vein-filling jadeite crystals and porphyroclastic jadeite crystals in the pale-greenish matrix, whereas no fluid inclusions were found in the fine-grained jadeites in the pale-greenish matrix.

METHODS

Color CL images of the New Idria jadeitite were obtained using a cold-type optical CL microscope (Nuclide model ELM-3R luminoscope) at the Okayama University of Science. This CL imaging system consists of an optical microscope attached with a cold-type electron gun and a Edmund Optics cooled charge-coupled device (CCD) camera. The optical CL microscopic observation was conducted at 15 kV accelerating voltage and 0.5 mA beam current. Owing to strong CL emissions from jadeitic clinopyroxene, adjustment gain value was set to low value ranging from 480 to 600.

CL spectral analysis of jadeites was conducted using a JEOL JSM-5410 scanning electron microscope (SEM) equipped with an Oxford Instruments Mono CL2 cathodoluminescence spectrometer at the Okayama University of Science. The CL spectra were measured ranging from 200 to 800 nm in 1 nm steps. The scanning electron microscope-cathodoluminescence (SEM-CL) was performed at 15 kV accelerating voltage and 0.70 nA beam current. All CL spectra obtained here were corrected for the total instrumental response, which was determined using a Eppley Laboratory quartz halogen lamp as calibrated standard. Based on the spectroscopic results, monochromatic high-resolution CL images were captured by using an Oxford/Gatan MiniCL imaging system with band-pass filters. The filtering ranges were selected from the results of the preliminary spectral measurements. In this study, high-resolution CL images in UV-blue and red emission regions were collected through the band-pass filters of 350 Fs at ~ 350 nm and 700 Fs at ~ 700 nm, respectively. The total instrumental response of a photomultiplier tube built in the MiniCL system has been reported in Kayama et al. (2010), where the maximum spectral response is at 400 nm, showing a smooth change from 200 to 800 nm.

Major-element composition (Si, Ti, Al, Cr, Fe, Mn, Mg, Ca, Na, and K) of jadeitic clinopyroxenes was determined using a JEOL JXA-8800R EPMA at Tohoku University. The quantitative analyses were performed with a 15 kV acceleration voltage, a 15 nA beam current and a 1 μm spot diameter. The oxide ZAF method was employed for matrix corrections, and natural and synthetic silicate and oxide minerals were used for calibrations as standards. The structural formulae of clinopyroxenes were calculated based on O = 6 and the Fe^{2+}/Fe^{3+} ratio was estimated based on four total cations. The end-member components of pyroxene were calculated by an algorithm suggested by Harlow (1999). Element distribution maps of Ti, Al, Fe, Mn, Mg, Ca, and Na were obtained with a 15 kV acceleration voltage and a 50 nA beam current.

RESULTS

CL microscopy

Color CL images of the New Idria jadeitite are shown in Figure 2. CL behaviors of the jadeitite can be divided into the dark and bright luminescent portions. Notably these dark and bright luminescent portions correspond to pale-greenish matrix and white veins of the jadeitite. In addition, the bright luminescent portions are composed of mixtures of red, blue and dull blue CL-colored domains. Such variations of the CL color and brightness reflect internal textures of the jadeite crystals, where the blue (or dull blue) CL-colored cores are overgrown by red CL-colored rims. Fine oscillatory growth bands, with rhythmic changes of red and (dull) blue CL, parallel to growth faces are also developed in internal texture of the bright luminescent portions. White veins that formed in the relatively older generations show no remarkable CL core-rim textures in the bright luminescent portion because of the deformation. In addition, porphyroclastic coarse-grained jadeite crystals and/or composite jadeite grains in the pale-greenish matrix emitted bright red and blue CL.

CL spectroscopy

CL spectra of the jadeites in white veins and pale-greenish matrix were examined by SEM-CL. CL spectra of nearly all jadeites consist of ultraviolet (UV)-blue and red emissions corresponding to two peaks centered at ~ 350 and ~ 700 nm. Representative CL spectra of the blue, dull blue and red CL-colored domains in a vein are shown in Figure 3. CL spectra of the blue, dull blue and red CL-colored domains commonly represent a doublet broad emission peak at ~ 320 and ~ 360 nm in the UV-blue regions. The blue CL-colored domains show high emission intensities of the UV-blue peak range, whereas the dull blue CL-colored domains show weak peak centered at ~ 360 nm (Fig. 3a). CL spectra of the dark luminescent portions of the pale-greenish matrix also have similar characteristics to

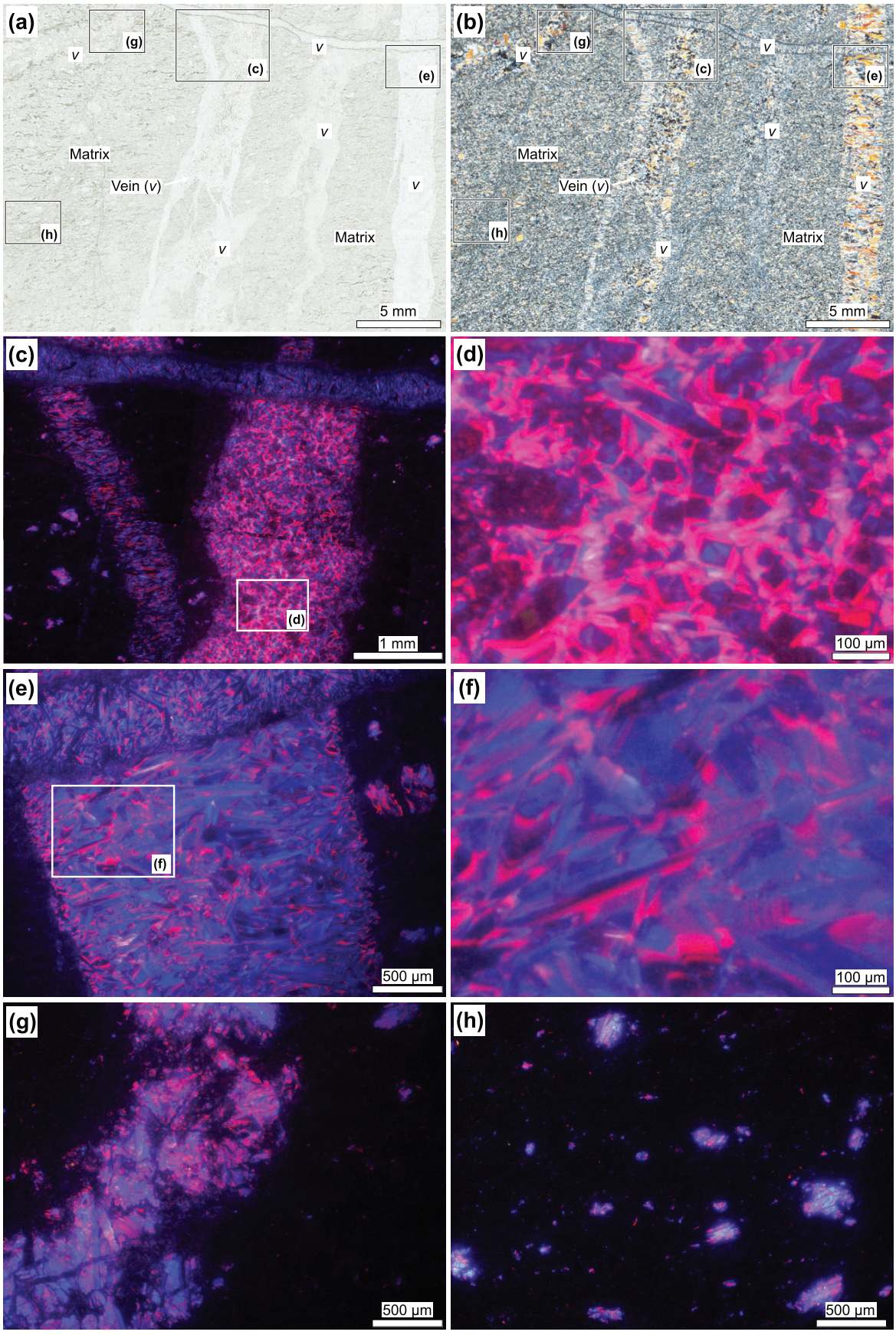
(a)
(g)
(c)
(e)
(h)
v
Matrix
Vein (v)
5 mm
(b)
5 mm
(c)
(d)
1 mm
(d)
100 μm
(e)
(f)
500 μm
(f)
100 μm
(g)
500 μm
(h)
500 μm

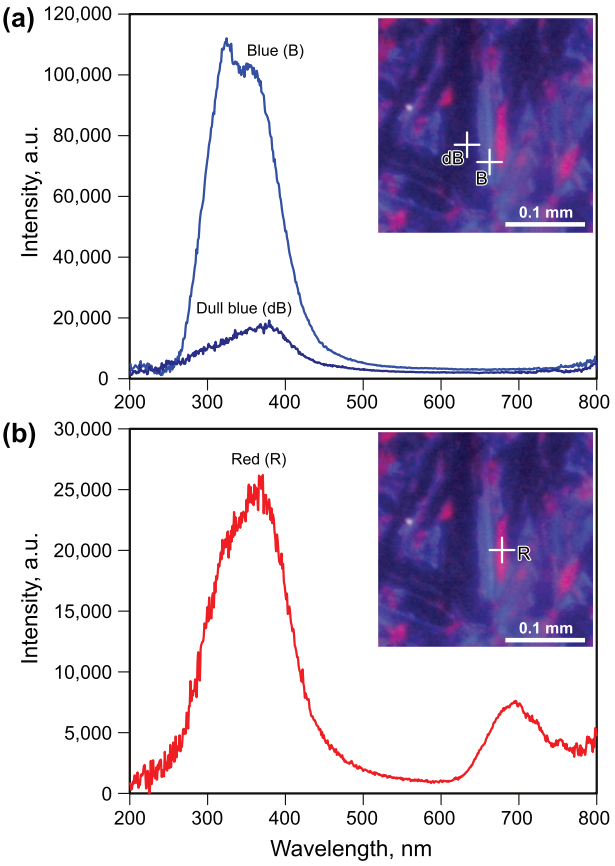

Figure 3. Cathodoluminescence (CL) spectra of selected spots of jadeite crystals from the New Idria jadeitite. (a) Blue (B) and dull blue (dB) CL-colored domains of jadeites. CL spectra show a doublet broad overlapping peaks at ~ 320 and ~ 360 nm. (b) Red (R) CL-colored domains of a jadeite. The spectrum is characterized by an additional peak at ~ 700 nm.

those of the dull blue CL-colored domains in the vein-filling jadeites. In the red CL-colored domain, an additional broad emission peak at ~ 700 nm was detected (Fig. 3b). Note that a red emission peak of one red CL-colored domain exhibits the exceptionally high intensity of ~ 70000 a.u., although all the other CL spectra are less than 20000 a.u. Based on these spectroscopic results, monochromatic high-resolution CL images in the UV-blue emission region (300-400 nm) and the red emission region (650-750 nm) were obtained. The images were used to compare with X-ray elemental maps as described in the next section.

Mineral compositions, elemental maps, and monochromatic CL images

Representative microprobe analyses are given in Table 1; all analyses are plotted in a ternary jadeite-augite-aegirine (Jd-Aug-Ae) diagram (Fig. 4) and a jadeite (Jd) versus multiple elements (CaO, FeO*, and MgO) diagram (Fig. 5). All our new compositional data of jadeitic pyroxenes characterized by optical CL overlap a compositional range that Tsujimori et al. (2007) randomly analysed the same sample. The pale-greenish matrix includes rare nearly pure jadeites, i.e. end-member jadeites, however overall it has significant impurities with a variable CaO (0.22 to 4.95 wt%) and FeO (0.12 to 5.37 wt%) (Jd_{72-95}). In contrast, vein-filling jadeites are mostly pure end-member composition (Jd_{97-100}), except for some dull blue CL-colored jadeites (Jd_{90-94}). EPMA analyses also confirmed that the jadeites of the red CL-colored domains had tended to contain higher Ca than those of the blue CL-colored domains, except for a nearly pure (Jd_{100}) red CL-colored jadeite (Table 1) with the highest intensity at ~700 nm peak. Hereafter we use terms 'pure' jadeite for vein-filling occurrence and 'impure' jadeite for matrix.

EPMA X-ray elemental maps of Ca and Fe (Figs. 6b and 6c) of oscillatory zoned vein-filling 'pure' jadeites (Fig. 6a) and the monochromatic red CL images through 650-750 nm wavelength (Fig. 6f) show a clear correlation between red CL intensity and minor Ca enrichment. In some cases, they also depend on subtle enrichment of Fe. It is noted that the domains with enrichment of Fe are characterized by very weak to dark emissions in the monochromatic UV-blue and red CL images, which is consistent with the dark luminescent portions under optical color CL microscopy. Moreover, both of the monochromatic UV-blue CL images through 300-400 nm (Fig. 6e) and red CL images are correlated with Al distribution, i.e., purity of jadeite component.

DISCUSSION

Textural and compositional constraints

The investigated jadeitite from the NISB is composed of

Figure 2. Optical images showing microtextures of the studied jadeitite. (a) Low magnification image of a polished thin-section, showing cross-cut relationships of white veins in pale-greenish jadeite matrix. (b) Crossed-polarized light view of (a). (c) CL image of a box (c) in (a). The white veins with bright luminescence (red, blue, and dull blue) are distinguished from the pale-greenish matrix with dark luminescence. (d) Enlarged image of a box (d) in (c), showing an internal texture of a white vein consisting of aggregates of jadeite. The jadeites show a distinct core (blue or dull blue)-rim (red) difference in CL. (e) CL image of a box (e) in (a). (f) Enlarged image of a box (f) in (e), showing an internal texture of a white vein, highlighting fine oscillatory growth bands in CL. (g) CL image of a box (g) in (a) of a partially-fragmented vein. Initial growth textures of jadeite crystals were modified irregularly by a deformation. (h) CL image of a box (h) in (a), showing fragments of coarse-grained jadeite crystals and/or composite jadeite grains (bright red and blue CL) in the fine-grained pale-greenish matrix with dark luminescence.

Table 1. Representative microprobe analyses of the investigated jadeitite (See details in text)

Spot#	1	2	3	4	5	6	7	8	9	10
Occurrence	Pale-greenish matrix			White vein-networks						
CL color	Dark			Red			Blue		Dull blue	
SiO_2	58.95	60.39	58.60	59.25	59.80	59.50	60.25	58.93	58.52	58.84
TiO_2	0.05	0.01	0.67	0.03	0.00	0.00	0.00	0.00	0.04	0.76
Al_2O_3	20.58	25.26	15.71	24.35	24.04	25.01	25.19	25.04	23.39	21.06
Cr_2O_3	0.04	0.00	0.00	0.03	0.01	0.00	0.00	0.00	0.03	0.03
FeO*	3.10	0.22	4.46	0.13	0.20	0.00	0.04	0.03	1.64	3.08
MnO	0.11	0.04	0.08	0.00	0.10	0.00	0.00	0.06	0.00	0.06
MgO	1.60	0.01	3.69	0.01	0.00	0.00	0.01	0.00	0.17	0.48
CaO	2.18	0.12	5.37	0.42	0.43	0.01	0.01	0.00	0.53	1.00
Na_2O	13.94	15.36	11.76	15.28	15.04	15.20	15.35	15.64	15.14	14.60
K_2O	0.01	0.00	0.01	0.00	0.00	0.00	0.00	0.00	0.01	0.00
Total	100.55	101.42	100.36	99.51	99.62	99.72	100.85	99.70	99.47	99.91
O= 6										
Si	2.003	2.005	2.030	2.008	2.022	2.006	2.009	1.993	1.994	2.012
Ti	0.001	0.000	0.017	0.001	0.000	0.000	0.000	0.000	0.001	0.020
Al	0.824	0.988	0.641	0.972	0.958	0.994	0.990	0.998	0.940	0.849
Cr	0.001	0.000	0.000	0.001	0.000	0.000	0.000	0.000	0.001	0.001
Fe^{3+}	0.085	0.000	0.055	0.004	0.000	0.000	0.000	0.001	0.047	0.056
Fe^{2+}	0.003	0.006	0.074	0.000	0.006	0.000	0.001	0.000	0.000	0.032
Mn	0.003	0.001	0.002	0.000	0.003	0.000	0.000	0.002	0.000	0.002
Mg	0.081	0.001	0.191	0.001	0.000	0.000	0.000	0.000	0.009	0.024
Ca	0.079	0.004	0.199	0.015	0.015	0.001	0.000	0.000	0.019	0.037
Na	0.919	0.989	0.790	1.004	0.987	0.993	0.992	1.026	1.001	0.968
K	0.000	0.000	0.001	0.000	0.000	0.000	0.000	0.000	0.000	0.000
Total	4.000	3.995	4.000	4.005	3.992	3.994	3.992	4.020	4.011	4.000
Jd, mol%	83.39	99.57	71.58	98.10	98.42	99.97	99.96	99.92	93.79	90.18
Ae, mol%	8.59	0.00	6.16	0.38	0.00	0.00	0.00	0.08	4.71	5.92
Aug, mol%	8.03	0.43	22.25	1.52	1.58	0.03	0.04	0.00	1.50	3.90

* Total iron as FeO

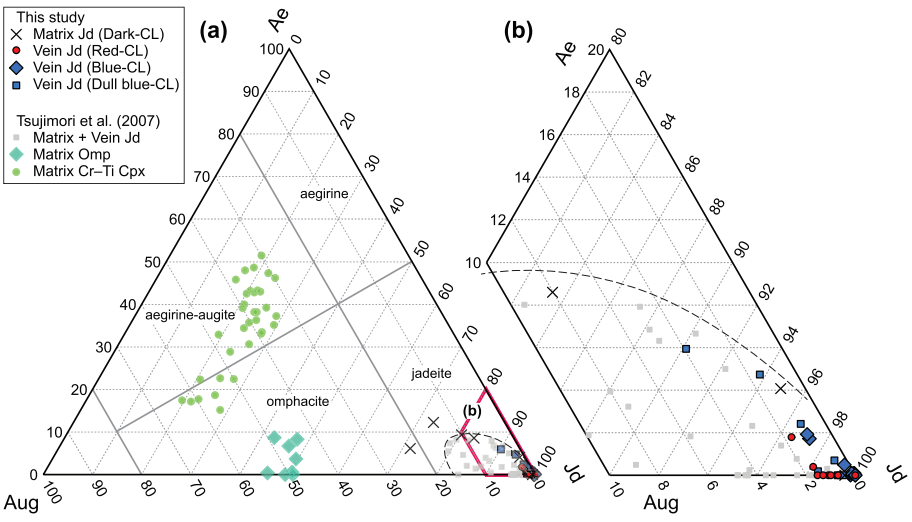

Figure 4. Compositions of clinopyroxenes. (a) Jd-Aug-Ae ternary diagram showing jadeite, omphacite, and Cr-Ti-rich clinopyroxene (Cr-Ti Cpx) in the New Idria jadeitite. (b) Enlarged image of a red trapezoid region in (a).

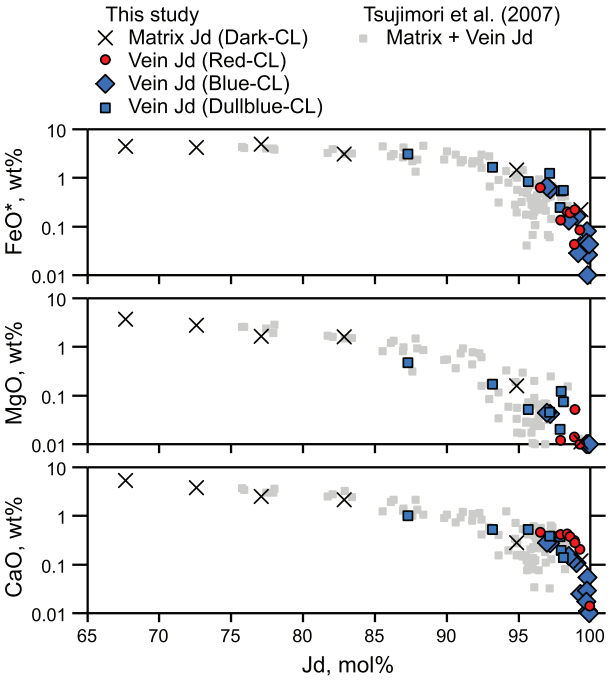

Figure 5. Jd versus multiple elements (CaO, FeO* and MgO) diagram.

pale-greenish matrix cut by multiple white veins. The vein-filling 'pure' jadeites show remarkable oscillatory zoning under optical CL microscopy, and contain abundant fluid inclusions. These textural features support an interpretation that multiple 'pure' jadeite veins are typical P-type (direct precipitation from aqueous fluids under high-pressure conditions) (Tsujimori and Harlow, 2012). In contrast, the pale-greenish matrix 'impure' jadeites have no textural evidence of fluid precipitation. More detailed petrogenesis of the New Idria jadeitite will be described elsewhere.

The 'impure' jadeites in the pale-greenish matrix exhibit dark luminescence, whereas 'pure' jadeites in the white veins show bright luminescence characterized by remarkable red and blue CL-colored emissions. As we described above, the 'impure' jadeites have significantly higher FeO component (up to 5.37 wt%), whereas the 'pure' jadeites are mostly close to an end-member composition. Therefore, we interpret that the contrasting CL brightness reflects quenching by Fe^{2+}, similar to the case of other zoned Fe^{2+}-bearing minerals such as olivine and feldspar (e.g., Marshall, 1988; Götze et al., 2000). Alternatively, it can be also possible due to the excess amount of Fe^{3+} as an activator, that is, concentration quenching as known in feldspar and calcite (Telfer and Walker, 1978; Habermann et al, 2000).

As Sorensen et al. (2006) showed in other jadeitite localities, it is difficult to distinguish the crystallization orders between red and blue CL-colored jadeites produced after the green CL-colored jadeites growth, because they have a characteristic mottled texture. However, the vein-filling 'pure' jadeites of the New Idria jadeitite are characterized by an initial crystallization of the blue CL-colored jadeites and subsequent overgrowth of the red CL-colored jadeites owing to their core-rim texture (see Figs. 2d and 2f). Such a sequential change in CL color variations of the New Idria jadeitite are closely related to types and concentrations of the luminescence centers as described below.

Assignment of luminescence centers

According to Dopfel (2006)'s preliminary study, CL of jadeite reflects some systematics, e.g., red emission intensity versus abundances of Al^{3+}, Ti^{4+}, Ca^{2+}, and REEs (Dy, Tm, and Gd), and blue emission intensity versus elemental abundances of Al^{3+} and Ti^{4+}. Our monochromatic UV-blue and red CL images of the New Idria jadeitite also show correlations of the brightness with Al^{3+} (purity of jadeite component). Our study also confirmed a good spatial correlation between red emission intensities and enrichments of Ca^{2+}. However, this is inconsistent with Dopfel (2006)'s observation, where the red emission intensity negatively correlates with Ca. It is noteworthy that less bright domains in both of the monochromatic UV-blue and red emissions correspond to Fe-enriched domains. This fact suggests that Fe^{2+} plays a role as quencher or excess amount of Fe^{3+} leads to concentration quenching.

CL spectra of the red CL-colored jadeites in energy units have asymmetric emission peaks in the regions corresponding to red wavelengths. If a spectral peak is assigned by only one luminescence center, it should be a symmetric shape (Kayama et al., 2010). However, the red emission peak of the 'pure' jadeite was asymmetric. This fact indicates that the red emission peaks of jadeites are composed of a mixture of multiple signals attributed to two or more luminescence centers. As we emphasized above, we confirmed an excellent spatial correlation between red emission intensities and enrichments of Ca^{2+}. In some red CL-colored domains, the similar correlations are also confirmed by the distribution of Fe^{2+} (or Fe^{3+}) without quenching of the emission. These features imply that a part of the luminescence centers of the red emission peak is assigned to be of lattice defects related to Ca^{2+}, and Fe^{2+} (or Fe^{3+}) or Mg^{2+} coupled with Ca^{2+} (intrinsic defect, but not extrinsic impurity centers), e.g., Ca^{2+}, Fe^{2+} (or Fe^{3+}) and Mg^{2+} deficiency and/or excess defect centers in M1 or M2 sites. Alternatively, the red emission peak is attributed to transition metal elements (Mn^{2+} and Fe^{3+}) and/or REEs impurities, substituting

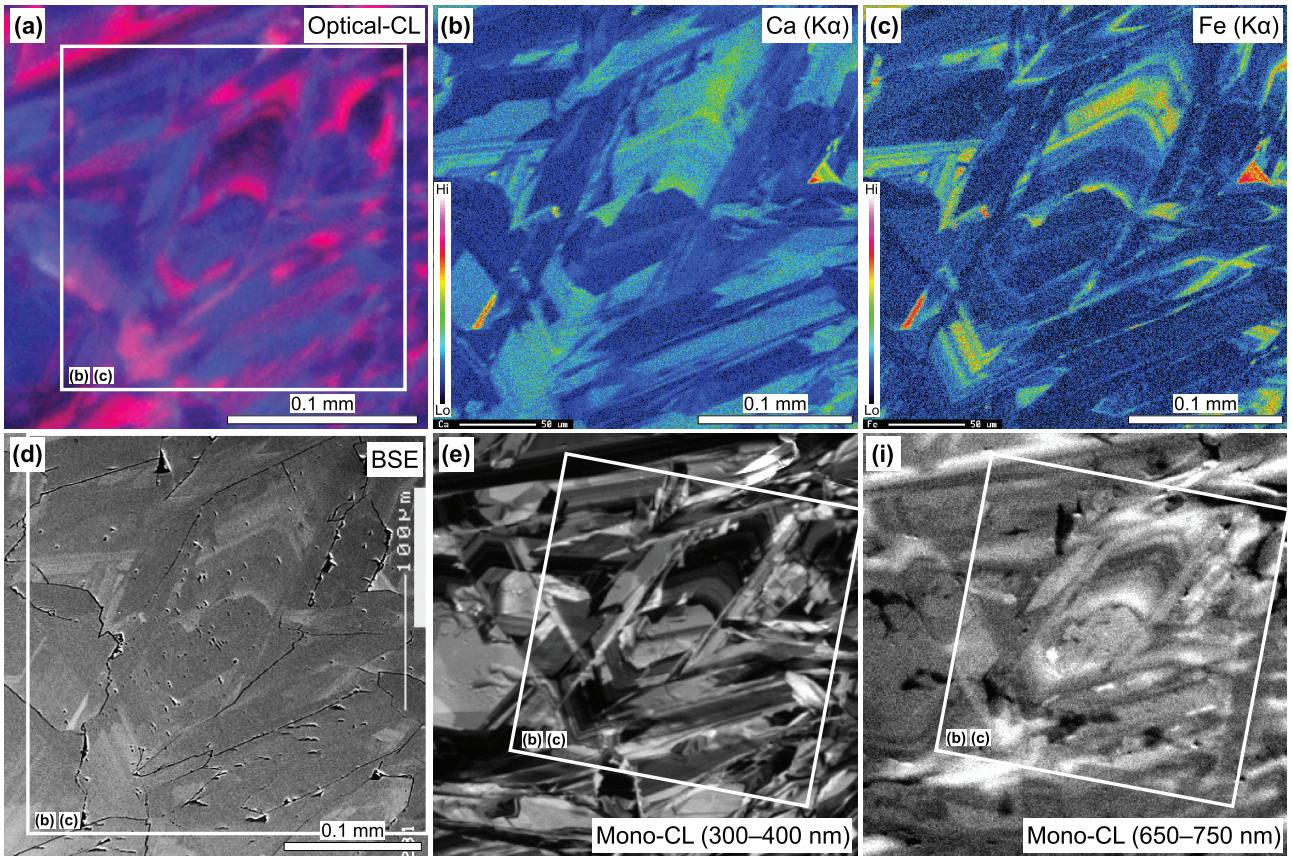

Figure 6. Comparisons of a zoned jadeite crystal in optical CL, X-ray elemental maps, BSE, and monochromatic CL images. (a) Optical CL image of a zoned jadeite crystal (center of the image), showing blue CL core mantled by an oscillatory zoned rim with bright red bands. (b) X-ray image of Ca showing enrichment of Ca and oscillatory zoning in the rim. (c) X-ray image of Fe showing a correlation of Fe and Ca as augite component. (d) BSE image of the zoned jadeite crystal showing an oscillatory zoning. (e) Monochromatic CL image in the 300-400 nm region. (f) Monochromatic CL image in the 650-750 nm region.

Ca^{2+}, or Fe^{2+} and Mg^{2+}, as extrinsic impurity centers. For example, Walker (2000) reported that a red emission peak of jadeite is due to Mn^{2+}. Moreover, Fe^{3+} also may play a role in substitution-type defect and impurity centers in quartz and feldspars (Steven-Kalceff, 2009; Kayama et al., 2011). Exceptionally, the jadeite with a highest intensity of the red emission peak was nearly pure end-member composition ($Jd_{99.9}$). Although this red emission cannot be explained by the luminescence centers as described above, the luminescence center of red emissions in the nearly pure end-member jadeite might imply the presence of other factors such as growth-induced lattice defect.

The UV-blue emission peak shows a doublet asymmetric shape in both wavelength and energy units. Therefore, two or more luminescence centers contribute to the UV-blue emission peak, same as in the case of the red emission peak of the jadeite. Our observations revealed that brightness of the monochromatic UV-blue CL image is correlated with abundance of Al^{3+} (i.e. purity of jadeite component); this is consistent with the results of Dopfel (2006), where Al^{3+} concentration correlates with the blue emission intensities of jadeite to some extent. We interpret that the UV-blue emissions peaks might be related to Na^{+} or Al^{3+} defect centers. According to Su et al. (2004), Na-rich jadeite can accommodate more OH than Na-poor jadeite. This suggests that the UV-blue emissions can be also featured by OH defects which are derivable under the assumption of M1, M2 and Si site vacancies in jadeite (Andrut et al., 2007). Actually, defect centers closely related to hydroxyl groups (e.g., nonbridging oxygen hole centers with OH precursor) have been also reported in CL of quartz (Steaven-Kalceff et al., 2000). However, there are no enough data of hydroxyl concentration in the New Idria jadeitite. In any case, CL microscopy and spectroscopy are the only techniques for an observation of the distribution of these luminescence centers (defects and impurities) with high-spatial resolutions. To further our understanding of the physico-chemical mechanism of CL in jadeite, a more detailed approach to transmission elec-

tron microscopy, trace-element and isotope geochemistry, and high-pressure experimental study is required than that documented in previous studies.

ACKNOWLEDGMENTS

We dedicate this paper to Dr. Sorena S. Sorensen who has addressed the significance of CL to study jadeitite. This research was supported by Center for Northeast Asian Studies, Tohoku University in part by grants from the MEXT/JSPS KAKENHI (15H05212) to T. Tsujimori. We also thank K. Ninagawa of the Okayama University of Science for his support to use SEM-CL facilities. We are grateful for constructive reviews from Y. Hiroi and K.E. Flores and constructive editorial evaluation from R. Miyawaki.

REFERENCES

Andrut, M., Wildner, M., Ingrin, J. and Beran, A. (2007) Mechanisms of OH defect incorporation in naturally occurring, hydrothermally formed diopside and jadeite. Physics and Chemistry of Minerals, 34, 543-549.

Atwater, B.F., Trumm, D.A., Tinsley III, J.C., Stein, R.S., Tucker, A.B., Donahue, D.J., Jull, A.J.T. and Payen, L.A. (1990) 15. Alluvial Plains and Earthquake Recurrence at the Coalinga Anticline. United States Geological Survey Professional Paper, 1487, 273.

Coleman, R.G. (1961) Jadeite deposits of the Clear Creek area, New Idria district, San Benito County, California. Journal of Petrology, 2, 209-247.

Coleman, R.G. (1986) Ophiolites and accretion of the North American Cordillera. Bulletin de la SocitéGéologique de France, 2, 961-968.

Cowan, D.S. and Mansfield, C.F. (1970) Serpentinite flows on Joaquin Ridge, southern coast ranges, California. Geological Society of America Bulletin, 81, 2615-2628.

Dopfel, E.C. (2006) The chemical activators of cathodoluminescence in jadeite, A thesis presented to the faculty of Mount Holyoke College in partial fulfillment of the requirements for the degree of Bachelor of Arts with Honor.

Götze, J., Krbetschek, M.R., Habermann, D. and Wold, D. (2000) High-resolution cathodoluminescence of feldspar minerals. In Cathodoluminescence in Geosciences (Pagel, M., Barbin, V., Blanc, P. and Ohnenstetter, D. Eds.). Springer Verlag, Berlin, 245-270.

Habermann, D., Neuser, R.D. and Richter, D.K. (2000) Quantitative high resolution spectral analysis of Mn^{2+} in sedimentary calcite. In Cathodoluminescence in Geosciences (Pagel, M., Barbin, V., Blanc, P. and Ohnenstetter, D. Eds.). Springer Verlag, Berlin, 331-358.

Harlow, G.E. (1999) Interpretation of Kcpx and CaEs components in clinopyroxene from diamond inclusions and mantle samples. In Proceedings of Seventh International Kimberlite Convention: Cape Town (Gurney, J.J. et al., Eds.). Redroof Design, 1, 321-331.

Kayama, M., Nakano, S. and Nishido, H. (2010) Characteristics of emission centers in alkali feldspar: A new approach by using cathodoluminescence spectral deconvolution. American Mineralogist, 95, 1783-1795.

Kayama, M., Nishido, H., Toyoda, S., Komuro, K. and Ninagawa, K. (2011) Combined cathodoluminescence and micro-Raman study of helium-ion-implanted albite. Spectroscopy Letters, 44, 526-529.

Marfunin, A.S. (1979) Spectroscopy, Luminescence and Radiation Centers in Minerals. pp. 352, Springer Verlag, Berlin.

Marshall, D.J. (1988) Cathodoluminescence of Geological Materials. Hyman, Boston.

Schertl, H.P., Maresch, W.V., Stanek, K.P., Hertwig, A., Krebs, M., Baese, R. and Sergeev, S.S. (2012) New occurrences of jadeitite, jadeite quartzite and jadeite-lawsonite quartzite in the Dominican Republic, Hispaniola: petrological and geochronological overview. European Journal of Mineralogy, 24, 199-216.

Sorensen, S., Harlow, G.E. and Rumble, D. (2006) The origin of jadeitite-forming subduction-zone fluids: CL-guided SIMS oxygen-isotope and trace-element evidence. American Mineralogist, 91, 979-996.

Steven-Kalceff, M.A. (2009) Cathodoluminescence microcharacterization of point defect in α-quartz. Mineralogical Magazine, 73, 585-605.

Steven-Kalceff, M.A., Phillips, M.R., Moon, A.R. and Kalceff, W. (2000) Cathodoluminescence microcharacterisation of silicon dioxide polymorphs. In Cathodoluminescence in Geosciences (Pagel, M., Barbin, V., Blanc, P. and Ohnenstetter, D. Eds.). Springer Verlag, Berlin, 193-224.

Su, W., Ji, Z., Ye, K., You, Z., Liu, J., Yu, J. and Cong, B. (2004) Distribution of hydrous components in jadeite of the Dabie Mountains. Earth and Planetary Science Letters, 222, 85-100.

Telfer, D.J. and Walker, G. (1978) Ligand field bands of Mn^{2+} and Fe^{3+} luminescence center and their site occupancy in plagioclase feldspars. Modern Geology, 6, 199-210.

Tsujimori, T., Liou, J.G. and Coleman, R.G. (2007) Finding of high-grade tectonic blocks from the New Idria serpentinite body, Diablo Range, California: Petrologic constraints on the tectonic evolution of an active serpentinite diapir. Geological Society of America Special Papers, 419, 67-80.

Tsujimori, T. and Harlow, G.E. (2012) Petrogenetic relationships between jadeitite and associated high-pressure and low-temperature metamorphic rocks in worldwide jadeitite localities: a review. European Journal of Mineralogy, 24, 371-390.

Vasyukova, O.V., Goemann, K., Kamenetsky, V.S., MacRae, C.M. and Wilson, N.C. (2013) Cathodoluminescence properties of quartz eyes from porphyry-type deposits: Implications for the origin of quartz. American Mineralogist, 98, 98-109.

Vermeesch, P., Miller, D.D., Graham, S.A., De Grave, J. and McWilliams, M.O. (2006) Multimethod detrital thermochronology of the Great Valley Group near New Idria, California. Geological Society of America Bulletin, 118, 210-218.

Walker, G. (2000) Physical parameters for the identification of luminescence centres in minerals. In Cathodoluminescence in Geosciences (Pagel, M., Barbin, V., Blanc, P. and Ohnenstetter, D. Eds.). Springer Verlag, Berlin, 23-39.

Yacobi, B.G. and Holt, D.B. (1990) Cathodoluminescence microscopy of inorganic solids. pp. 292. Plenum Press, New York.

Manuscript received April 3, 2017
Manuscript accepted July 6, 2017
Published online September 2, 2017
Manuscript handled by Ritsuro Miyawaki Guest Editor